

# A Simple Polarization-Recovery Algorithm for Dual-Polarized Cellular Mobile-Radio Systems in Time-Variant Faded Environments

Roberto Cusani, Enzo Baccarelli, Guido Di Blasio, and Stefano Galli

**Abstract**—Dual-polarized signaling constitutes an effective frequency-reuse technique to enhance the cell capacity in cellular mobile-radio systems. In the present paper, we present a new cross-polarization interference canceler (XPIC) which accomplishes the polarization-recovery task in time-division multiple-access (TDMA)-based cellular radio systems. The main new attractive feature of the proposed XPIC is that it is able to work even in the presence of unknown and possibly time-variant random phase fluctuations, as those due to imperfect phase recovery at the receiver side.

**Index Terms**—Dual-polarized radio transmission, cross-polarization interference, fading channels, maximum-likelihood parameter estimation.

## I. INTRODUCTION

**A**N EFFICIENT utilization of the limited bandwidth available for mobile-radio communications requires that effective frequency-reuse techniques be extensively exploited to increase the cell capacity and reduce the cluster size of the system [9, Sec. 9.5], [10, Sec. 7.6]. Dual-polarized data transmission constitutes an effective means to improve the spectral efficiency of cellular systems [1], [2] and its main features have been widely investigated in recent years (among other contributions on the subject, see, for example, [3]–[8] and references therein).

In dual-polarized cellular radio-systems a severe source of performance degradation is the cross-polarization interference (XPI). In fact, polarization orthogonality of the propagating field generally cannot be preserved in fading environments, so that the received signal is subject to depolarization effects [3]–[5] that can easily degrade the overall system performance, even in the absence of intersymbol interference (ISI) phenomena.

The design of optimum receivers handling XPI and ISI in a combined form so as to minimize the resulting system error probability has been widely investigated in literature, but a conclusive solution is yet to be found, mainly because of the non-Gaussian nature of ISI and XPI [3]. Feasible solutions to this problem can be obtained by separating the two tasks of XPI and ISI cancellation; to this regard, in [4] it has been shown that a receiver constituted by an XPIC followed by to an equalizer offers very good performances, besides providing modularity and

flexibility in the system design. However, the important results of [4] (such as those reported in [1]–[3], and [5]–[8]) have been derived under the *simplifying assumption* of a *perfect phase recovery* at the receiver side. On the other hand, for radio channels linking mobile units this assumption may be *overly optimistic*, because of the time-varying nature of the fading phenomena induced by the motion of the terminal units [9, ch. 2], [10, ch. 2].

In the present paper, starting from the usual channel model reported in [3]–[8], we propose an XPIC which performs the task of polarization-recovery by taking *explicitly* into account the effects of unknown and eventually time-variant phase fluctuations; furthermore, rough estimates of these phase fluctuations are also output by the proposed XPIC and can be utilized for a periodic restart of the phase-recovery unit (PRU) present in the receiver.

## II. MODELING OF DUAL-POLARIZED FADING-IMPAIRED RADIO LINKS

Let us consider the transmission of two orthogonally polarized  $M$ -ary QAM signals  $s_1(t)$  and  $s_2(t)$  sharing the same bandwidth and the same carrier. As it is well known [3], [5], the radio-frequency transmitted signal can be expressed as

$$S_i(t) \equiv \text{Re} \{ \tilde{s}_i(t) \exp(-j\omega_o t + \varphi) \}, \quad i = 1, 2 \quad (1)$$

where

$$\tilde{s}_i(t) \equiv \sum_{k=-\infty}^{\infty} \tilde{\alpha}_i(k) \tilde{h}(t - kT_s), \quad i = 1, 2 \quad (2)$$

is the complex envelope of  $S_i(t)$  and the  $i$  index refers to the two polarization components of the propagation field along the  $\vec{x}$  and  $\vec{y}$  axes. Furthermore

$$\{ \tilde{\alpha}_i(k) \equiv b_i(k) + jc_i(k) \in \mathcal{C}^1 \}, \quad i = 1, 2$$

in (2) is the sequence of the linearly polarized transmitted symbols which take values on an assigned (complex) two-dimensional (2-D) QAM constellation of size  $M$ ; as a consequence, the four real-valued terms  $b_1(k)$ ,  $c_1(k)$ ,  $b_2(k)$ ,  $c_2(k)$  individuate the data symbol of the resulting four-dimensional (4-D)  $M^2$ -QAM constellation transmitted at  $k$ th step. Finally,  $\tilde{h}(t)$  in (2) is the overall complex low-pass impulse response describing the cascade of the waveform channel and transmitting/receiving filters, whereas  $T_s$  is the signaling period.

Manuscript received October 14, 1997; revised August 31, 1998.

R. Cusani, E. Baccarelli, and G. Di Blasio are with the INFO-COM Department, University of Rome "La Sapienza," V 00184 Rome, Italy.

S. Galli is with Telcordia Technologies, Morristown, NJ 07960 USA.

Publisher Item Identifier S 0018-9545(00)00911-7.

Now, referring to a time-division multiple-access (TDMA) framing structure, let us assume as in [1]–[8] that the effects due to time-dispersive phenomena can be ignored, as it happens in satellite links and in land-mobile communications in rural and urban areas [9], [10]. In this case, a simple model for the received signal impaired by cross-polarization interference takes on the usual form (see, e.g., [5, eq. (3)])

$$\begin{aligned} \tilde{r}(t) &\equiv \begin{vmatrix} \tilde{r}_1(t) \\ \tilde{r}_2(t) \end{vmatrix} = \begin{vmatrix} a_{11} & a_{12} \\ a_{21} & a_{22} \end{vmatrix} \begin{vmatrix} \tilde{s}_1(t) \\ \tilde{s}_2(t) \end{vmatrix} + \begin{vmatrix} \tilde{w}_1(t) \\ \tilde{w}_2(t) \end{vmatrix} \\ &\equiv A\tilde{s}(t) + \tilde{w}(t) \end{aligned} \quad (3)$$

where  $\tilde{r}_1(t)$  and  $\tilde{r}_2(t)$  are the components of the received signal along the two axes  $\tilde{x}$  and  $\tilde{y}$ , respectively, and  $\tilde{w}_1(t)$ ,  $\tilde{w}_2(t)$  are (complex) mutually uncorrelated additive white Gaussian noise (AWGN) processes with known one-sided power-density spectra equal to  $N_o$  (W/Hz). The complex-valued coefficients  $a_{mn}$  ( $m, n = 1, 2$ ) are the channel parameters which describe the random amplitude attenuations (flat fading) and phase shifts introduced by the transmission link. Without loss of generality, let us now assume that the phases of the coefficients  $a_{11}$  and  $a_{22}$  are zero; so, by resorting to the following usual normalizations [5]–[8]:

$$\frac{a_{12}}{a_{11}} \equiv \xi_1 e^{j\psi_1} \quad \frac{a_{21}}{a_{22}} \equiv \xi_2 e^{j\psi_2} \quad \left| \frac{a_{11}}{a_{22}} \right| \equiv 1 \quad (4)$$

the channel matrix  $A$  of (3) can be equivalently rewritten in the normalized form

$$A \equiv \begin{vmatrix} 1 & \xi_1 e^{j\psi_1} \\ \xi_2 e^{j\psi_2} & 1 \end{vmatrix}. \quad (5)$$

The above matrix  $A$  is isomorphic to the  $4 \times 4$  real-valued channel matrix  $J$  defined as (see, e.g., [6, eq. (7)])

$$\begin{aligned} J &\equiv \begin{vmatrix} 1 & 0 & \xi_1 \cos \psi_1 & \xi_1 \sin \psi_1 \\ 0 & 1 & -\xi_1 \sin \psi_1 & \xi_1 \cos \psi_1 \\ \xi_2 \cos \psi_2 & \xi_2 \sin \psi_2 & 1 & 0 \\ -\xi_2 \sin \psi_2 & \xi_2 \cos \psi_2 & 0 & 1 \end{vmatrix} \\ &\equiv \begin{vmatrix} I_2 & \xi_1 \mathcal{R}(-\psi_1) \\ \xi_2 \mathcal{R}(-\psi_2) & I_2 \end{vmatrix} \end{aligned} \quad (6)$$

where  $I_2$  is the  $(2 \times 2)$  identity matrix and  $\mathcal{R}(\alpha)$  is the 2-D matrix rotation operator defined as

$$\mathcal{R}(\alpha) \equiv \begin{vmatrix} \cos \alpha & -\sin \alpha \\ \sin \alpha & \cos \alpha \end{vmatrix}. \quad (7)$$

On the basis of the above relationships, the baud-rate sampled<sup>1</sup> received signal can be expressed as (see, e.g., [6, eq. (3)])

$$r(k) = Jx(k) + w(k) \quad (8)$$

where the following positions hold for the real-valued four-variate vectors present in (8):

$$\begin{cases} r(k) \equiv [r_1(k), r_2(k), r_3(k), r_4(k)]^T \\ x(k) \equiv [x_1(k), x_2(k), x_3(k), x_4(k)]^T \\ w(k) \equiv [w_1(k), w_2(k), w_3(k), w_4(k)]^T \end{cases} \quad (9)$$

with the additional positions

$$\begin{aligned} \tilde{r}_1(t)|_{t=kT_s} &\equiv r_1(k) + jr_2(k) \\ \tilde{r}_2(t)|_{t=kT_s} &\equiv r_3(k) + jr_4(k) \\ \tilde{s}_1(t)|_{t=kT_s} &\equiv x_1(k) + jx_2(k) \\ \tilde{s}_2(t)|_{t=kT_s} &\equiv x_3(k) + jx_4(k) \\ \tilde{w}_1(t)|_{t=kT_s} &\equiv w_1(k) + jw_2(k) \\ \tilde{w}_2(t)|_{t=kT_s} &\equiv w_3(k) + jw_4(k). \end{aligned}$$

The channel model in (8) is the same considered in [1]–[6] and assumes a *perfect* coherent demodulation (that is, *perfect phase recovery*) at the receiver side. However, as already pointed out in Section I, this assumption generally falls short on frequency-dispersive channels as those encountered in mobile communications. So, a more realistic description of the mobile radio link requires that the above-mentioned overly optimistic assumption be discarded and that the following observation model be adopted:

$$\begin{aligned} r(k) &\equiv J\Phi(k)x(k) + w(k) \\ &= \begin{vmatrix} \mathcal{R}(\varphi(k)) & \xi_1 \mathcal{R}(\varphi(k) - \psi_1) \\ \xi_2 \mathcal{R}(\varphi(k) - \psi_2) & \mathcal{R}(\varphi(k)) \end{vmatrix} x(k) + w(k) \end{aligned} \quad (10)$$

where the four scalar components of the noise vector  $w(k)$  share a common known variance  $\sigma_N^2$  equal to  $(N_o/2)$  and the  $4 \times 4$  real unitary matrix

$$\Phi(k) \equiv \begin{vmatrix} \mathcal{R}(\varphi(k)) & 0 \\ 0 & \mathcal{R}(\varphi(k)) \end{vmatrix} \quad (11)$$

*explicitly models* the effects on the received signal of the randomly time-variant phase sequence  $\{\varphi(k)\}$  arising from imperfect phase recovery. Following [12] and its references, this random phase sequence can be adequately modeled as a discrete-time Wiener process, evolving according to the usual first order difference model

$$\varphi(k) = \varphi(k-1) + \Delta\varphi(k) \quad (12)$$

where the driving sequence  $\{\Delta\varphi(k)\}$  constitutes a white Gaussian noise with known variance  $\sigma_{\Delta\varphi}^2$  (rad<sup>2</sup>).

### III. THE PROPOSED CROSS-POLARIZATION INTERFERENCE CANCELER

The basic scheme of the proposed XPIC for TDMA-based radio-receivers is sketched in Fig. 1. In the data-aided operative mode (DA mode), the cross-polarization coefficients (XPC's)  $\xi_1, \xi_2, \psi_1, \psi_2$  previously introduced in (4) are periodically estimated on a per-frame basis by the XPC estimator (XPCE) via a slot header constituted by known symbols. In this way, the resulting estimated channel-matrix  $\hat{J}$  is built up and its inverse  $\hat{J}^{-1}$  is computed. So, in the following decided-data operative mode (DD mode), the product  $\hat{J}^{-1}r(k)$  is computed and then fed to a minimum Euclidean distance one-shot decision device that outputs the detected data vector  $\hat{x}(k)$ .

<sup>1</sup>We assume that perfect timing recovery is accomplished by the receiver so that the effects of timing jitters can be neglected in the discrete time channel-mode of (8). Several timing-recovery algorithms effective on fading channels which could be directly employed in the proposed receiver of Fig. 1 are described in [13].

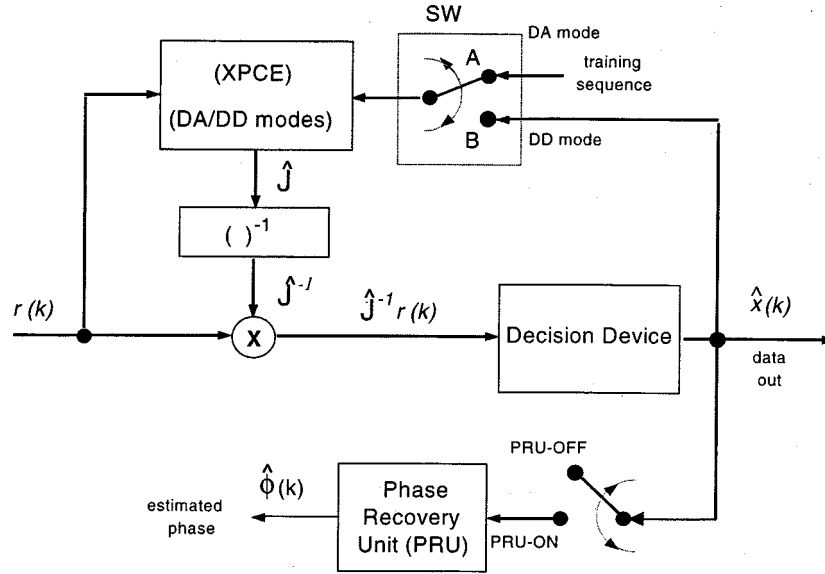


Fig. 1. Block diagram of the proposed receiver with the polarization recovery unit.

The presence of a header is typical for TDMA slots [10, ch. 1] where bursts of  $N$  symbols are constituted by  $L_p$  known symbols (the header) and  $(N - L_p)$  unknown data symbols. As it will be shown in the following sections, it is possible to estimate the XPC's  $\xi_1$  and  $\psi_1$  by transmitting  $L_p/2$  known symbols linearly polarized along the  $\vec{y}$  axis and then to estimate  $\xi_2$  and  $\psi_2$  by transmitting  $L_p/2$  known symbols linearly polarized along the  $\vec{x}$  axis. In the derivation of these XPC estimates, it is also assumed that the time fluctuations of the XPC's are negligible over a TDMA slot and this assumption can be considered approximately satisfied for values of the fading bandwidth  $B_D$  normalized to the symbol interval  $T_S$  (i.e., of the product  $B_D T_S$ ) of the order of  $10^{-4}$  when slots constituted by a few hundred symbols are transmitted (to this regard, see also the simulation results of Section V).

In the DA mode the switch SW in Fig. 1 is in the A position, the PRU is OFF and the decided data  $\hat{x}(k)$  are *not delivered* so that the computation of the product  $\hat{J}^{-1}r(k)$  is not carried out. At the end of the slot header, the XPC outputs the estimates of the XPC's and of the phase  $\varphi(k)$ ; this last estimate is then used to initialize the PRU of Fig. 1. At this point, the DD operative mode starts: the switch SW in Fig. 1 is routed to the B position and the PRU is turned ON; then, the PRU begins to track the time variant phase sequence  $\{\varphi(k)\}$  on the basis of the decided data  $\hat{x}(k)$  and the product  $\hat{J}^{-1}r(k)$  is computed to deliver the resulting detected stream  $\{\hat{x}(k)\}$ .

Since during the DD mode the PRU is ON, the resulting channel model is slightly different from that previously reported in (10); in fact, the PRU now computes the estimate  $\hat{\varphi}(k)$  of  $\varphi(k)$  on the basis of the decided symbol  $\hat{x}(k)$ , and then uses it to demodulate the received signal  $r(t)$  in the next signaling period [12]. Therefore, in the DD mode the channel model is given by the following relationship:

$$r(k) \equiv J\Phi_\varepsilon(k)x(k) + w(k) \\ = \begin{bmatrix} \mathcal{R}(\varphi_\varepsilon(k)) & \xi_1 \mathcal{R}(\varphi_\varepsilon(k) - \psi_1) \\ \xi_2 \mathcal{R}(\varphi_\varepsilon(k) - \psi_2) & \mathcal{R}(\varphi_\varepsilon(k)) \end{bmatrix} x(k) + w(k) \quad (13)$$

where  $\varphi_\varepsilon(k) \equiv \varphi(k) - \hat{\varphi}(k - 1)$  represents the one-step prediction error introduced by the PRU in the tracking of the phase fluctuation  $\varphi(k)$  [12].

The overall XPC estimation procedure carried out in the DA operative mode is described in detail in the following sections.

#### A. Estimation of the Channel Amplitude Coefficients $\xi_1$ and $\xi_2$ During the DA Mode

A simple and feasible procedure for estimating the amplitude coefficient  $\xi_2$  is based on the transmission of a known training sequence linearly polarized along the  $\vec{x}$  axis. In fact, since in this case we have:  $x(k) \equiv [x_1(k), x_2(k), 0, 0]^T$ , the received vector  $r(k)$  of (10) assumes the simplified form

$$r(k) \equiv \begin{bmatrix} r_{\vec{x}}(k) \\ r_{\vec{y}}(k) \end{bmatrix} = \begin{bmatrix} \mathcal{R}(\varphi(k))x_{\vec{x}}(k) \\ \xi_2 \mathcal{R}(\varphi(k) - \psi_2)x_{\vec{x}}(k) \end{bmatrix} + w(k) \quad (14)$$

where

$$x_{\vec{x}}(k) \equiv [x_1(k), x_2(k)]^T \\ r_{\vec{x}}(k) \equiv [r_1(k), r_2(k)]^T \\ r_{\vec{y}}(k) \equiv [r_3(k), r_4(k)]^T.$$

Now, although the parameter  $\xi_2$  is nonnegative [see (4)], its maximum likelihood (ML) estimate  $\hat{\xi}_2^{(ML)}$  may assume negative values especially during deeply faded transmission periods during which  $\xi_2$  is very close to zero [see (A2) of the Appendix]. As a consequence, we have experienced that, in practice, it is more robust to estimate  $(\xi_2)^2$  preliminarily and then obtain the corresponding estimate  $\hat{\xi}_2$  of  $\xi_2$  via a square-root operation. In fact, the square of the ML estimate  $\hat{\xi}_2^{(ML)}$  [computed on the basis of the received vector  $r_{\vec{y}}(k)$ ] assumes the simple nonnegative form below reported [see (A3) of the Appendix]

$$\left(\hat{\xi}_2^{(ML)}\right)^2 = \frac{r_{\vec{y}}^T(k)r_{\vec{y}}(k)}{E_p} \quad (15)$$

where  $E_p \equiv x_{\vec{x}}^T(k)x_{\vec{x}}(k)$  is the energy of the 2D-QAM  $k$ th training symbol. The estimate (15) is biased, but exploiting the

Gaussianity of the noise term  $w(k)$  in (14), the bias can be directly evaluated as

$$E \left\{ (\xi_2)^2 - \left( \hat{\xi}_2^{(\text{ML})} \right)^2 \right\} = -2 \frac{\sigma_N^2}{E_p} \quad (16)$$

and this term can be added to (15) so as to obtain an unbiased estimate of  $(\xi_2)^2$ . Exploiting the whiteness of the channel noise sequence  $\{w(k)\}$ , when a training sequence of  $N_\xi$  symbols polarized along the  $\vec{x}$  axis is transmitted, the overall estimate of the amplitude parameter  $(\hat{\xi}_2^{(\text{ML})})^2$  can be computed by averaging over the  $N_\xi$  partial estimates as below reported

$$\left( \hat{\xi}_2^{(\text{ML})} \right)^2 = \frac{1}{N_\xi} \sum_{j=1}^{N_\xi} \frac{r_{\vec{y}}^T(k-j)r_{\vec{y}}(k-j)}{E_p} - 2 \frac{\sigma_N^2}{E_p} \quad (17)$$

and the resulting nonnegative estimate  $\hat{\xi}_2$  directly arises from the positive square root of (17)

$$\hat{\xi}_2 = \sqrt{\frac{1}{N_\xi} \sum_{j=1}^{N_\xi} \frac{r_{\vec{y}}^T(k-j)r_{\vec{y}}(k-j)}{E_p} - 2 \frac{\sigma_N^2}{E_p}}. \quad (18)$$

Obviously, a dual procedure can be followed to estimate the channel parameter  $\xi_1$  when the transmitted training sequence is linearly polarized along the  $\vec{y}$  axis only. In fact, in this case the received vector  $r(k)$  of (10) assumes the simplified form

$$r(k) \equiv \begin{bmatrix} r_{\vec{x}}(k) \\ r_{\vec{y}}(k) \end{bmatrix} = \begin{bmatrix} \xi_1 \mathcal{R}(\varphi(k) - \psi_1) x_{\vec{y}}(k) \\ \mathcal{R}(\varphi(k)) x_{\vec{y}}(k) \end{bmatrix} + w(k) \quad (19)$$

with the position:  $x_{\vec{y}}(k) \equiv [x_3(k), x_4(k)]^T$  and the estimate of  $\xi_1$  can be directly computed as

$$\hat{\xi}_1 = \sqrt{\frac{1}{N_\xi} \sum_{j=1}^{N_\xi} \frac{r_{\vec{x}}^T(k-j)r_{\vec{x}}(k-j)}{E_p} - 2 \frac{\sigma_N^2}{E_p}} \quad (20)$$

where  $E_p \equiv x_{\vec{y}}^T(k)x_{\vec{y}}(k)$  is again the energy of the  $k$ th 2D-QAM transmitted training symbol.

As (18) and (20) point out, in order to compute  $\hat{\xi}_1$  and  $\hat{\xi}_2$  the term  $\sigma_N^2/E_p$  must be known. In cellular mobile systems, the reciprocal of this term (i.e., the received SNR) is, in general, periodically monitored (e.g., for handover purposes: see [9, ch. 10] and [10, ch. 8]); as an alternative, the algorithm developed *ad hoc* in [11] can be employed to estimate this parameter directly from the received data stream.

Due to the nonlinear forms exhibited by the (18) and (20), an analytical evaluation of the performance of the presented estimators appears a difficult task; however, extensive computer-simulations have shown that the obtained estimates are consistent for any values of the XPC's and of  $\sigma_{\Delta\varphi}^2$ . Some of the obtained numerical results are drawn in Fig. 2, where the variance of the estimation error on  $\xi_1$  is plotted versus its true value for several values of the parameter  $N_\xi$  and of the ratio  $E_p/N_o$ ; in the carried out simulations, the XPC's were generated as random variables with Rayleigh-distributed amplitude and uniform-distributed phase. As shown by the simulation results reported in Fig. 2, values of  $N_\xi$  ranging from five to ten generally give rise to reliable estimates of  $\xi_1$  and  $\xi_2$ .

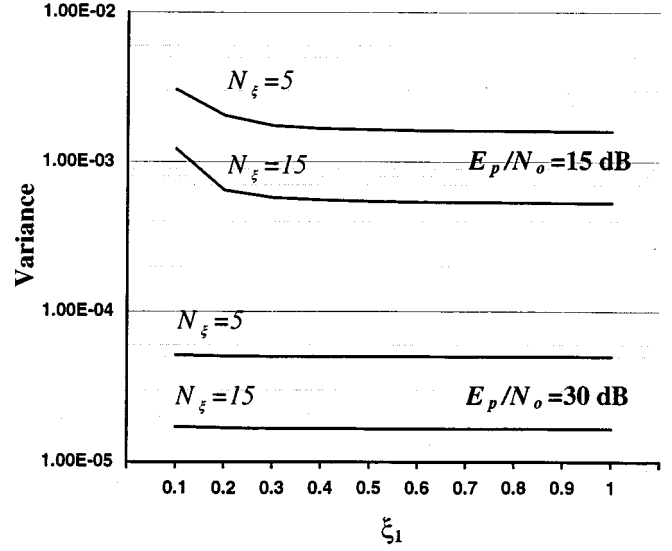


Fig. 2. Variance of the estimation error on  $\xi_1$  [with  $\hat{\xi}_1$  computed as in (20)] versus its true value, obtained via computer simulations for different lengths  $N_\xi$  of the training sequences and different values of  $E_p/N_o$ . The implemented modulation scheme is a 2-D 4-QAM with data transmissions transmitted linearly polarized along the  $\vec{y}$  axis. The presented simulation results are averaged on  $10^4$  independent trials. Similar curves (not reported here) have been obtained for the estimation error on  $\xi_2$ .

### B. Estimation of the Channel Phase Coefficients $\psi_1$ , $\psi_2$ , and $\varphi(k)$ During the DA Mode

From (14) we note that by transmitting a data stream linearly polarized along the  $\vec{x}$  axis we obtain information about the two phases  $\varphi(k)$  and  $\varphi(k) - \psi_2$ , while (19) points out that a data transmission polarized along the  $\vec{y}$  axis carries information about the two phases  $\varphi(k) - \psi_1$  and  $\varphi(k)$ . As a consequence, in order to estimate the three channel phase coefficients  $\psi_1$ ,  $\psi_2$ , and  $\varphi(k)$ , a training sequence with *both* polarization components should be, in principle, employed; indeed, we now show that, for this purpose, it is *sufficient* to transmit a training sequence linearly polarized along only one polarization axis at a time. In fact, when a symbol  $x(k)$  is transmitted linearly polarized along the  $\vec{x}$  axis we obtain the received vector  $r(k)$  of (14), so that the ML estimates  $\chi_1^{\vec{x}}(k)$ ,  $\chi_2^{\vec{x}}(k)$  of the phases of the bivariate subvectors  $r_{\vec{x}}(k)$  and  $r_{\vec{y}}(k)$  in (14) assume the following forms [see (A7) of the Appendix]:

$$\begin{aligned} \chi_1^{\vec{x}}(k) &\equiv \varphi(k) + \nu_{1x}(k) \\ &= \tan^{-1} \left[ \frac{r_{\vec{x}}(k)^T \mathcal{R}(\pi/2) x_{\vec{x}}(k)}{r_{\vec{x}}(k)^T x_{\vec{x}}(k)} \right] \end{aligned} \quad (21a)$$

$$\begin{aligned} \chi_2^{\vec{x}}(k) &\equiv \varphi(k) - \psi_2 + \nu_{2x}(k) \\ &= \tan^{-1} \left[ \frac{r_{\vec{y}}(k)^T \mathcal{R}(\pi/2) x_{\vec{x}}(k)}{r_{\vec{y}}(k)^T x_{\vec{x}}(k)} \right]. \end{aligned} \quad (21b)$$

The above ML estimates are *unbiased* and *asymptotically efficient*. For high SNR's the estimation errors  $\nu_{1x}(k)$ ,  $\nu_{2x}(k)$  present in (21a), (21b) can be approximately modeled as zero-mean Gaussian random variables with variances equal to  $\sigma_{\nu_{1x}}^2 = \sigma_N^2/E_p$  and  $\sigma_{\nu_{2x}}^2 = \sigma_N^2/(\xi_2^2 E_p)$ , respectively. Now, on the basis of the above estimates  $\chi_1^{\vec{x}}(k)$  and  $\chi_2^{\vec{x}}(k)$ , we can

directly compute the corresponding estimates for  $\varphi(k)$  and  $\psi_2$  as in the following:

$$\begin{aligned} \hat{\psi}_2(k) &\equiv \chi_1^{\bar{x}}(k) - \chi_2^{\bar{x}}(k) \equiv \psi_2 + e_2(k), \\ &\text{with } e_2(k) \equiv \nu_{1x}(k) - \nu_{2x}(k) \end{aligned} \quad (22a)$$

$$\hat{\varphi}(k) \equiv \chi_1^{\bar{x}}(k) \equiv \varphi(k) + \nu_{1x}(k). \quad (22b)$$

A dual procedure can be followed to estimate  $\psi_1$  by transmitting symbols linearly polarized along the  $\bar{y}$  axis; in fact, the ML estimates  $\chi_1^{\bar{y}}(k)$ ,  $\chi_2^{\bar{y}}(k)$  of the phases of the vectors  $r_{\bar{x}}(k)$  and  $r_{\bar{y}}(k)$  of (19) take on the forms below reported (see the Appendix)

$$\begin{aligned} \chi_1^{\bar{y}}(k) &\equiv -\psi_1 + \varphi(k) + \nu_{1y}(k) \\ &= \tan^{-1} \left[ \frac{r_{\bar{x}}(k)^T R(\pi/2) x_{\bar{y}}(k)}{r_{\bar{x}}(k)^T x_{\bar{y}}(k)} \right] \end{aligned} \quad (23a)$$

$$\begin{aligned} \chi_2^{\bar{y}}(k) &\equiv \varphi(k) + \nu_{2y}(k) \\ &= \tan^{-1} \left[ \frac{r_{\bar{y}}(k)^T R(\pi/2) x_{\bar{y}}(k)}{r_{\bar{y}}(k)^T x_{\bar{y}}(k)} \right]. \end{aligned} \quad (23b)$$

For high SNR's the estimation errors  $\nu_{1y}(k)$  and  $\nu_{2y}(k)$  can again be considered zero-mean and Gaussian, with variances equal to  $\sigma_{\nu_{1y}}^2 = \sigma_N^2 / (\xi_1^2 E_p)$  and  $\sigma_{\nu_{2y}}^2 = \sigma_N^2 / E_p$ , respectively. Therefore, on the basis of the above two ML estimates  $\chi_1^{\bar{y}}(k)$  and  $\chi_2^{\bar{y}}(k)$  we can obtain estimates for  $\varphi(k)$  and  $\psi_1$  as in the following:

$$\begin{aligned} \hat{\psi}_1(k) &\equiv \chi_2^{\bar{y}}(k) - \chi_1^{\bar{y}}(k) = \psi_1 + e_1(k), \\ &\text{with } e_1(k) \equiv \nu_{2y}(k) - \nu_{1y}(k) \end{aligned} \quad (24a)$$

$$\hat{\varphi}(k) \equiv \chi_2^{\bar{y}}(k) = \varphi(k) + \nu_{2y}(k). \quad (24b)$$

Hence, by averaging the partial estimates reported in (22a) and (24a) over  $N_\psi$  symbols linearly polarized along the  $\bar{x}$ - and  $\bar{y}$ -axes, we obtain the formulas below reported for the overall ML estimates of  $\psi_1$  and  $\psi_2$

$$\begin{aligned} \hat{\psi}_1 &= \frac{1}{N_\psi} \sum_{j=0}^{N_\psi-1} [\chi_2^{\bar{y}}(k-j) - \chi_1^{\bar{y}}(k-j)] \\ &\equiv \psi_1 + e_{1N} \end{aligned} \quad (25a)$$

$$\begin{aligned} \hat{\psi}_2 &= \frac{1}{N_\psi} \sum_{j=0}^{N_\psi-1} [\chi_1^{\bar{x}}(k-j) - \chi_2^{\bar{x}}(k-j)] \\ &\equiv \psi_2 + e_{2N}. \end{aligned} \quad (25b)$$

The random variables  $e_{1N}$  and  $e_{2N}$  in (25a) and (25b) are the resulting estimation errors; for high SNR's, these errors can be again modeled as zero-mean Gaussian random variables with variances given by the following expressions:

$$\sigma_{e_{1N}}^2 = \frac{1}{N_\psi} \frac{\sigma_N^2}{E_p} \left( 1 + \frac{1}{\xi_1^2} \right) \quad (26a)$$

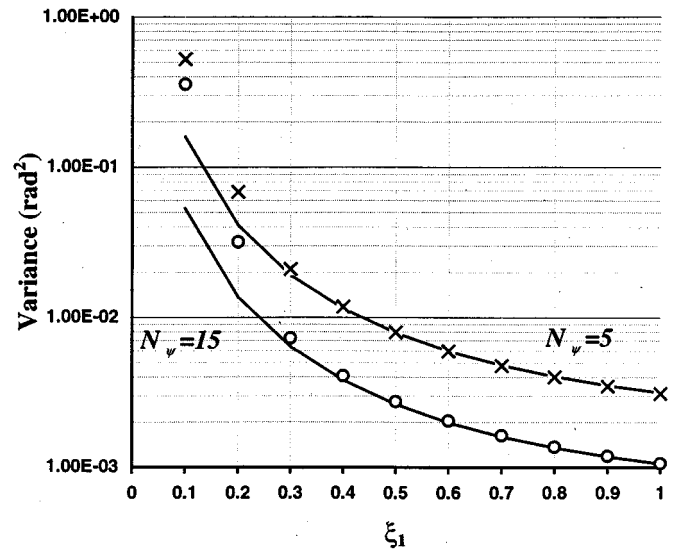


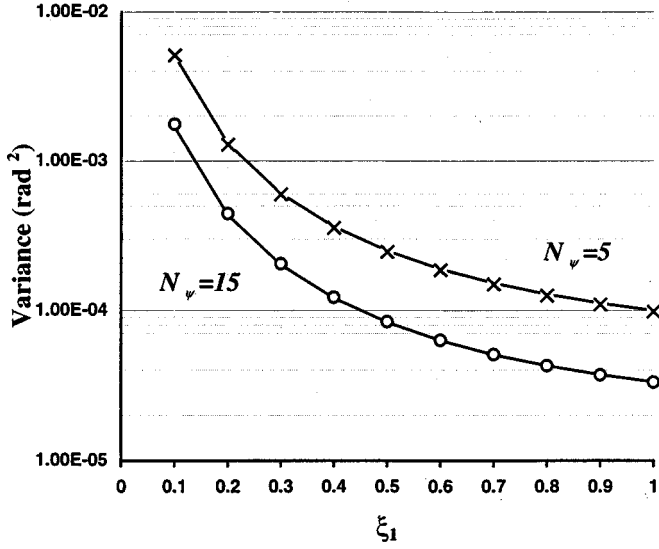
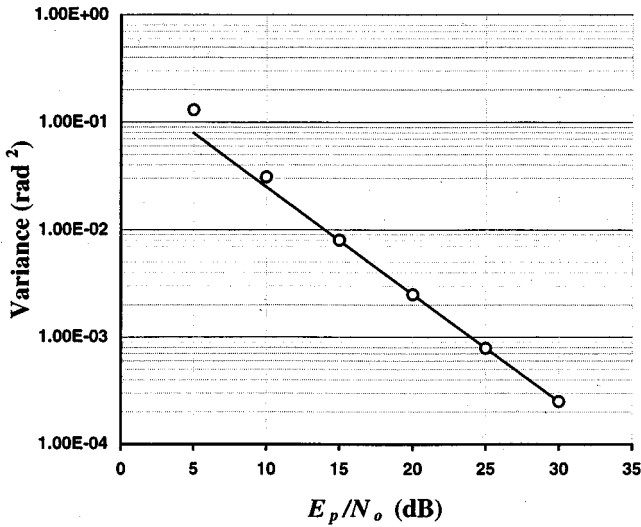
Fig. 3. Variance (rad<sup>2</sup>) of the estimation error on  $\psi_1$ , with  $\hat{\psi}_1$  as in (26a) (solid lines) versus the true value of  $\xi_1$  for training sequences of lengths  $N_\psi = 5$  and  $N_\psi = 15$  symbols and  $E_p/N_o = 15$  dB. Simulation results (indicated by crosses and circles) are also reported and have been obtained by averaging on 10<sup>4</sup> independent trials. The implemented modulation scheme is a 2-D 4-QAM with data transmissions linearly polarized along the  $\bar{y}$  axis. Similar curves (not reported here) have been obtained for the variance of the estimation error on  $\psi_2$ .

$$\sigma_{e_{2N}}^2 = \frac{1}{N_\psi} \frac{\sigma_N^2}{E_p} \left( 1 + \frac{1}{\xi_2^2} \right). \quad (26b)$$

Equations (26a) and (26b) point out that the performance of the estimators in (25a) and (25b) depends on the value assumed by the amplitude coefficients  $\xi_1$  and  $\xi_2$  so that when  $\xi_1$  ( $\xi_2$ ) vanishes the variance of the estimation error of  $\psi_1$  ( $\psi_2$ ) should, in principle, approach infinity. However, this *does not constitute* a drawback because (6) shows that, when  $\xi_1$  ( $\xi_2$ ) vanishes, the value assumed by  $\psi_1$  ( $\psi_2$ ) is not relevant. As a consequence, substantial errors in the estimation of  $\psi_1$  ( $\psi_2$ ) *do not at all affect* the overall system performance when  $\xi_1$  ( $\xi_2$ ) vanishes: this constitutes an attractive feature of the proposed polarization-recovery algorithm in deeply faded environments.

The relationships in (22b) and in (24b) also give rise to (rough) estimates of the channel-phase fluctuation  $\varphi(k)$  in (12) which can be fed to the PRU of Fig. 1 for a periodic restart of the phase estimation algorithm. To this regard, we remark that the estimate of the channel phase  $\varphi(k)$  must be computed on the basis of one observation only; in fact, since  $\varphi(k)$  is time variant, its estimates (22b) and (24b) *cannot* be averaged over multiple signaling periods as for  $\psi_1$  and  $\psi_2$  in (25a) and (25b).

In order to test the effectiveness of the phase estimator in (25a), in Figs. 3 and 4 the corresponding error variance (26a) is plotted versus the true value assumed by the parameter  $\xi_1$  and some simulation results are also added for convalidation purposes; moreover, in Fig. 5 the variance of the estimation error on  $\varphi(k)$  is also plotted, with the estimate  $\hat{\varphi}(k)$  computed at the end of each header slot according to (21a) and (22b). The simulation results reported in Figs. 3–5 were obtained generating the XPC's as random variables with Rayleigh-distributed amplitude and uniform-distributed phase.

Fig. 4. The same as in Fig. 3 at an  $E_p/N_o$  of 30 dB.Fig. 5. Behavior of the variance (rad<sup>2</sup>) of the estimation error on  $\varphi(k)$  with  $\hat{\varphi}(k)$  given by (24b). Simulation results (crosses) have been obtained by averaging on  $10^4$  independent trials. The implemented modulation scheme is a 2-D 4-QAM with data transmissions linearly polarized along the  $\vec{y}$  axis.

#### IV. COMPUTATIONAL BURDEN OF THE PROPOSED XPIC

The computational burden of the proposed XPIC estimators is here analyzed in terms of both arithmetical complexity (products/divisions and sums/subtractions) and memory requirements.

For the computation of each partial estimate in (15), two products ( $P$ ) and one addition ( $S$ ) are carried out on a per-symbol basis; the partial estimates so obtained are stored in an accumulator. At the end of the  $N_\xi$  training symbols,  $(N_\xi - 1)$  sums and one product are performed for the averaging and, finally, an additional sum and a lookup table operation  $L$  are carried out to obtain the final estimate in (18); furthermore, one memory cell is needed to store this final estimate. Therefore, the overall number of real operations needed to compute the estimate of  $\xi_2$

as in (18) is equal to  $(3N_\xi + 1)P + 2N_\xi S + L$ . The same computational burden is requested to calculate the corresponding estimate of  $\xi_1$  in (20).

As far as the estimates of  $\psi_1$  and  $\psi_2$  in (25a) and (25b) is concerned, it is convenient to obtain them by transmitting QAM symbols cited at the corners of the two 2-D subconstellations constituting the overall employed 4-D constellation, so as to minimize the estimation error variances of (26a) and (26b). In this case, the vector  $x_{\vec{x}}(k)$  of (21a) and (21b) and the vector  $x_{\vec{y}}(k)$  of (23a) and (23b) share the form  $x_{\vec{x}}(k) = x_{\vec{y}}(k) = C[1 \ 1]^T$ , where  $C$  is a known gain factor depending on the maximum energy allowed to the 2D-QAM transmitted symbols. The argument of the  $\tan^{-1}$  function present in the relationship (21a) then boils down to the following simpler form:  $[(r_2(k) - r_1(k))/(r_1(k) + r_2(k))]$ , and similar expressions are obtained for the relationships reported in (21b), (23a), and (23b). Therefore, for the computation of  $\chi_1^{\vec{x}}(k)$  and  $\chi_2^{\vec{x}}(k)$  as in (21a) and (21b),  $P + 2S$  real-valued operations are required to calculate the argument of the  $\tan^{-1}$  function, plus one lookup table operation  $L$  to compute the  $\tan^{-1}$  function; an additional summation  $S$  is needed to compute  $\hat{\psi}_2$  as in (22a). The total number of real operations per symbol required to compute  $\psi_2$  as in (22a) amounts to  $2P + 5S + 2L$ . After receiving the  $N_\psi$  training symbols,  $(N_\psi - 1)$  sums and one product must be performed for the averaging; so, the overall number of real operations needed to compute the estimate in (25b) amounts to  $(2N_\psi + 1)P + (6N_\psi - 1)S + 2N_\psi L$  and the same computational burden is requested to calculate the estimate in (25a).

Once the XPC's are estimated during the DA mode, the matrix  $\hat{J}^{-1}$  must be computed (see Fig. 1). However, in actual implementations of the proposed XPIC it is *not necessary* to explicitly carry out the inversion of  $\hat{J}$ ; in fact,  $\hat{J}^{-1}$  can be directly expressed in a closed form as in the following:

$$\hat{J}^{-1} \equiv \frac{1}{\det(\hat{J})} \cdot \begin{vmatrix} I_2 - \hat{\xi}_1 \hat{\xi}_2 \mathcal{R}(\hat{\psi}_1 + \hat{\psi}_2) & \hat{\xi}_1^2 \hat{\xi}_2 \mathcal{R}(\hat{\psi}_2) - \hat{\xi}_1 \mathcal{R}(-\hat{\psi}_1) \\ \hat{\xi}_1 \hat{\xi}_2^2 \mathcal{R}(\hat{\psi}_1) - \hat{\xi}_2 \mathcal{R}(-\hat{\psi}_2) & I_2 - \hat{\xi}_1 \hat{\xi}_2 \mathcal{R}(\hat{\psi}_1 + \hat{\psi}_2) \end{vmatrix} \quad (27)$$

where  $\det(\hat{J}) \equiv 1 + \hat{\xi}_1^2 \hat{\xi}_2^2 - 2\hat{\xi}_1 \hat{\xi}_2 \cos(\hat{\psi}_1 + \hat{\psi}_2)$ . The total number of real-valued operations needed to build matrix (27) at the end of the DA mode amounts to:  $31P + 7S + 11L$ ; in fact, only six elements among the 16 of matrix (27) must be explicitly computed since matrix (27) presents the following simple structure:

$$\hat{J}^{-1} \equiv \begin{vmatrix} a & -b & c & -d \\ b & a & d & c \\ e & -f & a & -b \\ f & e & b & a \end{vmatrix}. \quad (28)$$

Finally, during the DD mode, the products  $\hat{J}^{-1}r(k)$  must be carried out on a per symbol basis so as to generate the input of the decision device (see Fig. 1); the computational burden requested by this operation is equal to  $16P + 12S$  per received symbol.

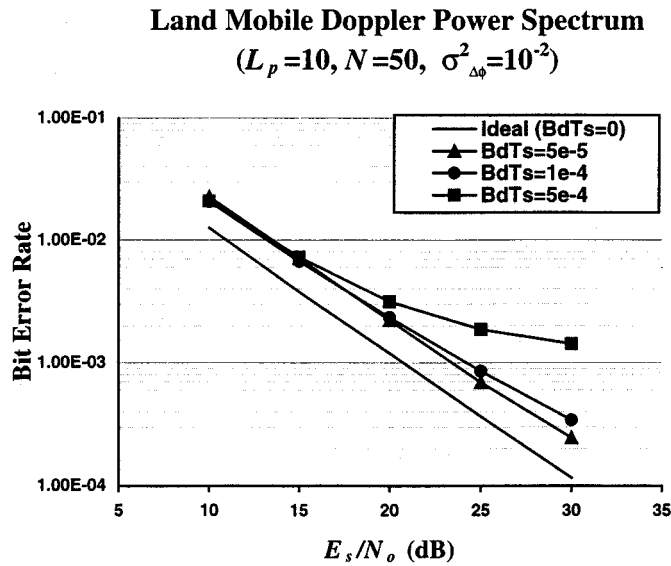


Fig. 6. BER performance of the overall receiver in Fig. 1. The generated XPC sequences are Rayleigh-distributed in amplitude with uniform distributed phases and their random fluctuations are modeled according to the Land Mobile Doppler power spectrum reported in (29). The random phase fluctuations have been generated according to (12) with a variance  $\sigma_{\Delta\varphi}^2$  of  $10^{-2}$  rad<sup>2</sup>. The transmitted TDMA slot is  $N = 50$  symbols long and the training sequence is constituted by  $L_p = 10$  symbols. As a benchmark, the BERS obtained for the ideal case of perfect estimation of the XPC's and perfect phase recovery are also plotted for vanishing  $B_D T_S$  (solid line).

#### V. PERFORMANCE ANALYSIS OF THE PROPOSED RECEIVER AND CONCLUSIVE REMARKS

The performance of the proposed receiver of Fig. 1 has been tested via computer simulations in terms of bit error rate (BER) versus SNR. Obviously, the ultimate performance of the receiver also depends on the particular algorithm adopted to track the phase fluctuations  $\{\varphi(k)\}$ . In our simulations, we have implemented the PRU described in [12] which was *ad hoc* developed for 4D-QAM constellation formats; it consists of a decision-driven hybrid-type PLL which implements a Kalman-like tracker that recursively outputs the minimum mean square error estimates of the random phase fluctuations  $\{\varphi(k)\}$  of (12) (see [12] for more details on the implemented phase estimator).

In the carried out simulations, the receiver of Fig. 1 periodically switches between the DA and the DD mode according to the procedure described as follows.

- 1) *DA Mode*: At the beginning of each TDMA slot, a known training sequence of  $L_p/2$  symbols linearly polarized along the  $\vec{x}$  axis followed by a known training sequence of  $L_p/2$  symbols linearly polarized along the  $\vec{y}$  axis is transmitted. The switch SW is in the A position and the PRU is OFF (see Fig. 1). The channel amplitude coefficient  $\xi_2$  is estimated as in (18) and the phase coefficient  $\psi_2$  is estimated as in (25b) on the basis of the training symbols transmitted linearly polarized along the  $\vec{x}$  axis only [i.e.,  $N_\xi = L_p/2$  in (18) and  $N_\psi = L_p/2$  in (25b), respectively]. Afterwards, the channel amplitude coefficient  $\xi_1$  is estimated as in (20) and the phase coefficient  $\psi_1$  is estimated as in (25a) on the basis of the training symbols transmitted linearly polarized along the  $\vec{y}$  axis only [i.e.,  $N_\xi = L_p/2$  in (20) and  $N_\psi = L_p/2$  in

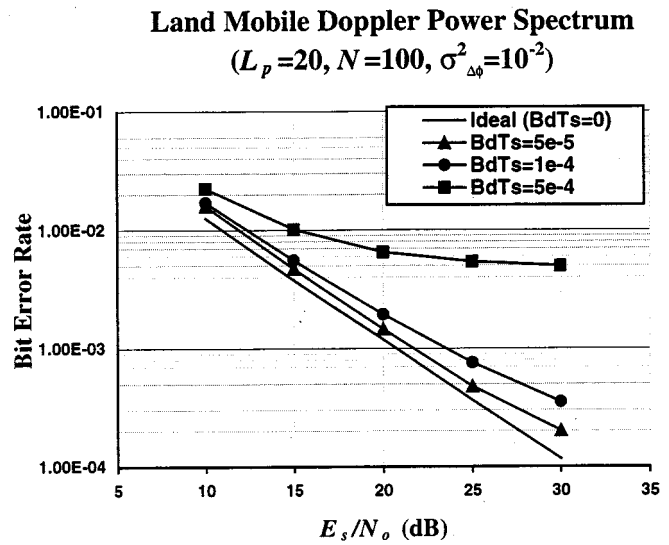


Fig. 7. The same as in Fig. 6, for  $L_p = 20$  and  $N = 100$ .

(25a), respectively]. At this point, estimates of  $\varphi(k)$  are also available from (22b) and (24b). Since such estimates share the same variance, the criterion for the selection of the best estimate of  $\varphi(k)$  for initializing the PRU is to use the *more recent* available estimate; this implies that (22b) must be employed when the last training symbol is transmitted linearly polarized along the  $\vec{x}$  axis and (24b) otherwise.

- 2) *DD Mode*: Having received the  $L_p$ -long training sequence, the inverse  $\hat{J}^{-1}$  of the estimated channel matrix  $\hat{J}$  is computed according to (27); the PRU is turned ON and initialized by the above-mentioned estimate of  $\varphi(k)$ . The receiver of Fig. 1 is now ready to detect the information-stream which is constituted by the remaining  $(N - L_p)$  unknown symbols of the transmitted TDMA slot.

The simulation results reported in Figs. 6–8 show the performance of the receiver of Fig. 1 (when the proposed XPIC is used) in terms of BER's versus the SNR expressed as  $E_S/N_o$ , where  $E_S$  is the energy of the transmitted 4-D symbol. In the carried out simulations, XPC's with Rayleigh-distributed amplitude and uniform-distributed phase are generated as time-variant random sequences exhibiting the usual land mobile doppler power spectrum [9, eq. (1.1)], [10, eq. (2.22)]

$$S_D(f) = \frac{1}{\pi B_D \sqrt{1 - \left(\frac{f}{B_D}\right)^2}}, \quad |f| \leq B_D. \quad (29)$$

In order to test the robustness of the proposed XPIC against the channel-parameter fluctuations, values of the product  $B_D T_S$  ranging from zero to five  $\cdot 10^{-4}$  have been considered.

The reported performance plots show that the performance penalty due to the assumption of time-invariant XPC's on a TDMA slot is generally small for channels exhibiting values of  $B_D T_S$  up to  $10^{-4}$ . Moreover, from the simulation results it can also be noted that using slots with  $N = 100$  yields slightly better performances than those obtained using  $N = 50$  for

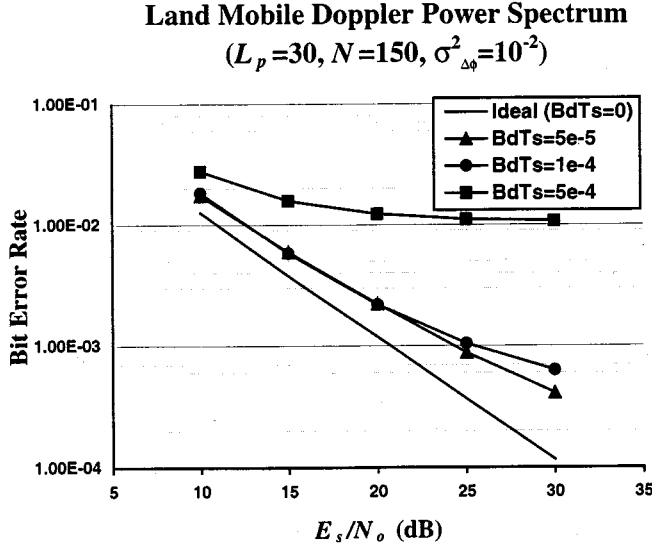


Fig. 8. The same as in Fig. 6 for  $L_p = 30$  and  $N = 150$ .

values of  $B_D T_S$  up to  $10^{-4}$  (see Figs. 6 and 7); in fact, in this case the channel can be considered virtually time invariant for values of  $N$  up to 100, so that longer slot headers allow the XPCE to generate more reliable estimates of the XPC's thus improving system performances. On the contrary, when  $B_D T_S$  is larger than  $10^{-4}$ , better performances are generally obtained for smaller values of the TDMA slot length  $N$ . In fact, in this case the impairments arising from the time variations of the channel parameters overcome the gain due to the higher reliability of the XPC's estimates achieved via longer slot headers.

In conclusion, the reported simulation results support the effectiveness of the presented polarization-recovery procedure for dual polarized TDMA-based cellular mobile-radio systems affected by time-variant fading phenomena. In fact, the obtained results indicate that the proposed XPIC allows the receiver to perform accurate XPI cancellation even in the presence of unknown and time-variant random phase fluctuations, thus giving rise to good performances of the overall resulting system.

## APPENDIX

### ESTIMATION OF THE XPC'S

#### A. Derivation of (15)

Taking into account that  $w_{\bar{y}}(k)$  is a Gaussian white sequence, the logarithmic ML equation for the estimation of  $\xi_2$  assumes the form below reported

$$\left[ r_{\bar{y}}(k) - \hat{\xi}_2^{(\text{ML})} \mathcal{R}(\varphi(k) - \psi_2) x_{\bar{x}}(k) \right]^T \mathcal{R}(\varphi(k) - \psi_2) x_{\bar{x}}(k) = 0. \quad (\text{A1})$$

By noting that  $(\mathcal{R}(\alpha))^T = R(-\alpha)$ , from (A1) we derive the following expression for the ML estimate of  $\xi_2$ :

$$\begin{aligned} \hat{\xi}_2^{(\text{ML})} &= \frac{r_{\bar{y}}^T(k) \mathcal{R}(\varphi(k) - \psi_2) x_{\bar{x}}(k)}{E_p} \\ &= \xi_2 + \frac{w_{\bar{y}}^T(k) \mathcal{R}(\varphi(k) - \psi_2) x_{\bar{x}}(k)}{E_p}. \end{aligned} \quad (\text{A2})$$

Squaring both sides of (A2) we directly obtain (15), that is,

$$\begin{aligned} \left( \hat{\xi}_2^{(\text{ML})} \right)^2 &= \frac{r_{\bar{y}}^T(k) r_{\bar{y}}(k)}{E_p} \\ &\equiv (\xi_2)^2 + \frac{1}{E_p} \left[ w_{\bar{y}}^T(k) w_{\bar{y}}(k) + 2\xi_2 x_{\bar{x}}^T(k) \right. \\ &\quad \left. \cdot \mathcal{R}(-\varphi(k) + \psi_2) w_{\bar{y}}^T(k) \right]. \end{aligned} \quad (\text{A3})$$

#### B. Derivation of (21a), (21b), (23a), and (23b)

When a training sequence polarized only along the  $\bar{x}$  axis is transmitted, the received sequence is [see (14)]

$$r_{\bar{x}}(k) = [\cos \varphi I_2 + \sin \varphi \mathcal{R}(\pi/2)] x_{\bar{x}}(k) + w_{\bar{x}}(k). \quad (\text{A4})$$

Now, taking into account that  $w_{\bar{x}}(k)$  is Gaussian and white, the ML equation (in the logdomain) for the estimate  $\hat{\varphi}_{\text{ML}}(k)$  of the phase sequence  $\varphi(k)$  assumes the following form [for the sake of simplicity, we drop the index  $k$  from  $\hat{\varphi}_{\text{ML}}(k)$ ]

$$\begin{aligned} [r_{\bar{x}}(k) - [\cos \hat{\varphi}_{\text{ML}} I_2 + \sin \hat{\varphi}_{\text{ML}} \mathcal{R}(\pi/2)] x_{\bar{x}}(k)]^T \\ \cdot [-\sin \hat{\varphi}_{\text{ML}} I_2 + \cos \hat{\varphi}_{\text{ML}} \mathcal{R}(\pi/2)] x_{\bar{x}}(k) = 0. \end{aligned} \quad (\text{A5})$$

So, by noting that

$$[-\sin \hat{\varphi}_{\text{ML}} I_2 + \cos \hat{\varphi}_{\text{ML}} \mathcal{R}(\pi/2)] = R(\hat{\varphi}_{\text{ML}} + \pi/2)$$

the term

$$\begin{aligned} \{ [\cos \hat{\varphi}_{\text{ML}} I_2 + \sin \hat{\varphi}_{\text{ML}} \mathcal{R}(\pi/2)] x_{\bar{x}}(k) \}^T \\ \cdot [-\sin \hat{\varphi}_{\text{ML}} I_2 + \cos \hat{\varphi}_{\text{ML}} \mathcal{R}(\pi/2)] x_{\bar{x}}(k) \end{aligned}$$

in (A5) vanishes since it represents the dot product between the two orthogonal vectors  $\mathcal{R}(\hat{\varphi}_{\text{ML}}) x_{\bar{x}}(k)$  and  $\mathcal{R}(\hat{\varphi}_{\text{ML}} + \pi/2) x_{\bar{x}}(k)$ . Therefore, (A5) can be rewritten as

$$r_{\bar{x}}^T(k) [-\sin \hat{\varphi}_{\text{ML}} I_2 + \cos \hat{\varphi}_{\text{ML}} \mathcal{R}(\pi/2)] x_{\bar{x}}(k) = 0 \quad (\text{A6})$$

and, after some standard algebra, we obtain the following relationship for  $\tan \hat{\varphi}_{\text{ML}}$ :

$$\tan \hat{\varphi}_{\text{ML}} = \frac{r_{\bar{x}}^T(k) \mathcal{R}(\pi/2) x_{\bar{x}}(k)}{r_{\bar{x}}^T(k) x_{\bar{x}}(k)}. \quad (\text{A7})$$

The last formula leads directly to the ML estimate  $\hat{\chi}_2^{\bar{x}}(k) = \hat{\varphi}_{\text{ML}}(k)$  of the phase  $\varphi(k)$  reported in the relationship (21a). The expressions for  $\hat{\chi}_2^{\bar{x}}(k)$ ,  $\hat{\chi}_1^{\bar{y}}(k)$ , and  $\hat{\chi}_2^{\bar{y}}(k)$  are obtained in a similar way.

#### ACKNOWLEDGMENT

The authors would like to thank two anonymous reviewers for their helpful suggestions.

#### REFERENCES

- [1] M. Takahashi, H. Takanashi, and T. Tanaka, "Cross polarization interference canceler for microcellular mobile communication systems," in *Int. Conf. Commun., ICC'95*, June 1995, pp. 910–914.
- [2] Y. Nagashima, Y. Ogawa, M. Ohmiya, and K. Itoh, "Interference cancellation in dual digital land mobile communications," *IEICE*, vol. J73-B-II, no. 11, pp. 745–754, 1990.

- [3] M. Kavehrad and J. Salz, "Cross-polarization cancellation and equalization in digital transmission over dually polarized multipath fading channels," *AT&T Bell Lab. Tech. J.*, vol. 64, no. 10, pp. 2211–2245, Dec. 1985.
- [4] L. J. Greenstein, "Analysis/simulation study of cross-polarization cancellation in dual-polarization digital radio," *AT&T Bell Lab. Tech. J.*, vol. 64, no. 10, pp. 2261–2280, Dec. 1985.
- [5] M. Kavehrad, "Performance of cross-polarized  $M$ -ary QAM signals over nondispersive fading channels," *AT&T Bell Lab. Tech. J.*, vol. 63, pp. 499–521, Mar. 1984.
- [6] M. Kavehrad, P. J. McLane, and C. E. Sundberg, "On the performance of combined quadrature amplitude modulation and convolutional codes for cross-coupled multidimensional channels," *IEEE Trans. Commun.*, vol. 34, pp. 1190–1201, Dec. 1986.
- [7] S. T. Hsieh, K. V. Cartwright, P. F. Duvoisin, and E. P. Williamson, "A comparison of three diagonalizers, adaptive crosstalk cancellers, in dual-polarized  $M$ -QAM system," *IEEE Trans. Commun.*, vol. 39, pp. 930–933, Mar. 1991.
- [8] S. T. Hsieh, K. V. Cartwright, P. F. Duvoisin, and E. P. Williamson, "Correction to 'A comparison of three diagonalizers, adaptive crosstalk cancellers, in dual-polarized  $M$ -QAM system'," *IEEE Trans. Commun.*, vol. 39, p. 1411, Sept. 1991.
- [9] G. L. Stüber, *Principles of Mobile Communications*. Norwell, MA: Kluwer, 1996.
- [10] R. Steele, *Mobile Radio Communications*. London, U.K.: Pentech, 1992.
- [11] R. Cusani and E. Baccarelli, "Parameter identification of frequency-selective noisy fast-fading Rayleigh digital channels via nonlinear Yule–Walker like equations," in *Proc. VIII Europ. Sign. Proc. Conf. (EUSIPCO'96)*, Trieste, Italy, Sept. 10–13, 1996, pp. 2001–2004.
- [12] R. Cusani, E. Baccarelli, and A. Salonic, "Recursive carrier phase tracking for synchronous multilevel 4QAM receivers," *IEEE J. Lightwave Technol.*, vol. 13, pp. 1655–1662, Aug. 1995.
- [13] K. E. Scott and E. B. Olasz, "Simultaneous clock phase and frequency offset estimation," *IEEE Trans. Commun.*, vol. 43, pp. 2263–2270, July 1995.

**Roberto Cusani** was born in Rome, Italy, in 1957. He received the "laurea" degree in electronic engineering and the Ph.D. degree in communication theory from the University of Rome "La Sapienza," Rome, in 1981 and in 1986, respectively.

In 1985, he was a Visiting Researcher at the Politechnical School of Lausanne, Switzerland. In 1986, he was a Research Engineer at the University of Rome "Tor Vergata," teaching digital signal processing. In 1991, he joined the University of Rome "La Sapienza," where currently he is an Associate Professor of Signal Theory. He also teaches communications at the University of L'Aquila, Italy. His former research activities were in the areas of statistical signal processing, both in one and in two dimensions, with particular emphasis on random processes, spectral estimation, and image coding. His current interests are mainly focused on digital communication systems, with particular emphasis on channel equalization and coding for radio-mobile links. He holds a U.S. patent in adaptive equalization of radio channels.

**Enzo Baccarelli** was born in Todi, Italy, in 1962. He received the "laurea" degree in electronic engineering and the Ph.D. degree in communication theory from the University of Rome "La Sapienza," Rome, Italy, in 1989 and in 1993, respectively.

In 1995, he carried out the "postdoctorate" course at the INFOCOM Department, University of Rome "La Sapienza," Rome, and, in 1996, became a Researcher. Currently, he is an Associate Professor at the INFOCOM Department, where he teaches communications. His main research activities are in the areas of random processes and information theory, with applications to the radio-mobile digital communications and coding. He holds a U.S. patent in adaptive equalization of radio channels.

**Guido Di Blasio**, photograph and biography not available at the time of publication.

**Stefano Galli** was born in Florence, Italy, on January 7, 1966. He received the "Laurea" degree in electronic engineering and the Ph.D. degree in information theory and communications from the University of Rome "La Sapienza," Rome, Italy, in 1994 and 1998, respectively.

His first research interests were on coherent optical communications; while he was a Ph.D. candidate at the INFOCOM Department, University of Rome "La Sapienza," his interests moved to digital communications. After completing his Ph.D., he continued his research activity at the INFOCOM Department and began to work as a free consultant. In October 1998, he joined Telcordia Technologies, Morristown, NJ, as a Research Scientist. His major research areas are in digital communications, with particular emphasis on channel equalization and coding for radio-mobile links.